High Accuracy Scattering Center Modeling Based on PO and PTD

Xiao-Tong ZHAO, Kun-Yi GUO, Xin-Qing SHENG

Center for Electromagnetic Simulation, School of Information and Electronics Beijing Institute of Technology, 5 South Zhongguancun Street, Haidian District, Beijing, 100081, P.R. China

ttmovingcastle@qq.com, guokunyi, xsheng@bit.edu.cn

Submitted December 4, 2017 / Accepted May 3, 2018

Abstract. *Based on the solutions of physical optics (PO) and physical optics of diffraction (PTD), we propose a modified parametric scattering center model for high precise signal simulations of extended targets. Different from geometrical theory of diffraction (GTD), which is commonly used in the existing models, the solution of PTD represents the individual scattering contribution of edge diffraction, and can precisely describe the scattering field under full observation angles and polarizations. This model has higher precision than the existing ones, especially for the targets with dominant scattering centers induced by diffraction. And this model is physical where the parameters are related with geometry of the targets. To validate this model, four conducting targets with dominant contributions of diffraction are simulated in this study. The radar cross-sections (RCS) and the time-frequency representations (TFR) of backscattered waves simulated by this model are compared with those computed by a full-wave numerical method, as well as those simulated by a commonly used scattering model. The comparisons show that the results of this model have better agreement with those of the full-wave numerical method than the existing model.*

Keywords

Scattering center model, physical optics (PO), physical optics of diffraction (PTD), edge diffraction, radar cross-sections (RCS)

1. Introduction

At high frequencies, the scattering response of an object can be described as the sum of responses from individual scattering centers [1]. Many scattering center models [2–7] are exploited to provide parametric descriptions of scattering characteristics of targets, and they are widely applied in the area of radar, such as radar image interpretation, automatic target recognition and geometry reconstruction [8–13].

The existing scattering center models are generally derived from the scattering solutions of canonical objects by high-frequency methods. For example, the commonly used attribute scattering center model (ASC model) introduces the term $(\mathrm{j}k)^{\alpha}$ according to solutions of geometry theory of diffraction (GTD) as frequency dependency expressions, and the sinc function according to solutions of physical optics (PO) as aspect dependency expressions [3]. However, the solutions of GTD actually contain both surface and edge contributions, in other words, PO and physical optics of diffraction (PTD) contributions [14].

The parametric model for each type of scattering centers is based on its unique scattering mechanism. Hence, the combination of the GTD and PO solutions results in repeated descriptions of reflection contributions in scattering center modeling. In comparison of GTD, the solution of PTD includes only edge diffraction. PTD is generally applied together with PO to describe the total scattering fields. Besides, considering the singular problems of GTD, the observation range should be separated into specular zone and diffraction zone in scattering center modeling. However, there is no obvious boundary for the two zones, which brings much disadvantage in scattering center modeling.

A scattering center modeling approach based on solutions of PO and PTD instead of PO and GTD is used in this work. More specifically, we introduce the formula of EEC to build the parametric model for edge diffraction rather than the solution of GTD which is commonly used in the existing methods. The benefit of doing this is that the problems induced by the singularities of GTD and the duplicated scattering components in the solutions of PO and GTD are avoided. Compared with the existing parametric model, this model further includes the dependent function on azimuth angle under two polarizations, VV and HH. And the expression for HH polarization has better agreement with the numerical results computed by the full wave method than the original EEC formula.

To verify these models, four conducting targets are investigated in detail: a plane, two propellers and a wing of an unmanned aerial vehicle (UAV).These targets are selected here for they all have dominant scattering center induced by diffraction contributions. The scattered fields simulated

by these models were compared with those computed by parallel-multilevel fast multiple algorithm (PMLFMA) [16], as well as those simulated by the ASC model. The results demonstrate that these models have higher precision in simulating both radar cross-section (RCS) and time-frequency representation (TFR) than the ASC model. As an important mean for scattering center analysis, TFR has been widely used in the study of various target characteristics [5–7,17]. The method of TFR used in this work is the Wigner-Ville distribution (RSPWVD) [18].

2. Scattering Center Models Derived Based on PO and PTD

2.1 The Scattering Center Model for Edge Diffraction

The solution of EEC for an edge of a conducting half-plane is investigated firstly. The geometry of the edge (highlighted by a red line) on the half-plane is shown in Fig. 1(a). A local coordinate system (x,y,z) is used to describe the geometry of the half-plane. To simplify the expressions, scalar scattering fields under two co-polarizations are presented.

Referring to Fig. 1(a), the vertical (VV) polarization means that electric field (**E**) is parallel to the edge and the horizontal (HH) polarization, meaning that **E** is perpendicular to the edge. The diffracted fields by the edge under plane wave incidence can be computed by a integration of the equivalent current over the edge [19]. And the integration results under different polarizations are derived as given below:

$$E^d_{\mathrm{V,H}} = \frac{\mathrm{e}^{-\mathrm{j}kr}}{\pi r} L F_{\mathrm{V,H}}(\theta,\phi)\,\mathrm{sinc}(2kL\cos\theta)\mathrm{e}^{2\mathrm{j}k\hat{s}\cdot\mathbf{r}'} \quad (1)$$

where k is the wave number; r is the distance between the radar and the origin of the local coordinate system; θ, ϕ are elevation and azimuth angles of the unit vector of the line of sight (LOS) with respect to the center of the edge; L is the half length of the edge; $\hat{s}$ is the unit vector of LOS; $\mathbf{r}'$ is the location of the center of the edge.

In the case of Fig. 1, $\mathbf{r}' = 0$. The expressions for $F_{\mathrm{V,H}}(\theta,\phi)$ for different polarizations are:

$$F_{\mathrm{V}}(\theta,\phi) = \frac{\sqrt{2}\sin\frac{\phi}{2}}{\cos\phi - \cot^2\theta}\left(\sqrt{1-\mu} - \sqrt{2}\cos\frac{\phi}{2}\right), \quad (2)$$

$$F_{\mathrm{H}}(\theta,\phi) = \frac{\sin\phi}{\cos\phi - \cot^2\theta}\left[1 - \frac{\sqrt{2}\cos(\frac{\phi}{2})}{\sqrt{1-\mu}}\right] \quad (3)$$

where $\mu = \cos\phi - 2\cot^2\theta$.

In order to give a concise form of these formulas, we analyse the aspect dependences on θ and ϕ of (2) and (3) by a series of numerical experiments. First, for the given geometry setting, only the rays which are near Keller's cone contribute to the backscattered waves, that is, only when θ approaches to $\frac{\pi}{2}$, the diffracted rays contributes to the backscattered fields. The backscattered waves under other elevation angles are too weak to be observed. Therefore, the observation angles within $|\theta - \frac{\pi}{2}| < \arccos(\frac{\pi}{kL})$, are only considered in scattering center modeling.

Then, we give an investigation on the term $\sqrt{1-\mu}$ in detail. In (2), as the part of numerator, the $2\cot^2\theta$ can be approximated to be zero. The dependency of E^d_{V} on θ can be approximated precisely by $\mathrm{sinc}(2kL\cos\theta)$; the dependency of $F_{\mathrm{V}}(\theta,\phi)$ on ϕ can be approximated as a simpler expression as given below. However, in (3), as part of the denominator, when the value of $1-\cos\phi$ is close to zero, even a tiny change of the value in $2\cot^2\theta$ will cause a large change in the computation results. So (3) cannot be simplified as (2). According to the numerical results computed by PMLFMA, the value of θ in (3) is modified to $\theta + \triangle\theta$. The modified $F_{\mathrm{V,H}}(\theta,\phi)$ is described by:

$$F_{\mathrm{V}}(\phi) = \frac{1-\cos\phi - |\sin\phi|}{\cos\phi}, \quad (4)$$

$$F_{\mathrm{H}}(\phi,\theta) = \tan\phi\left[1 - \frac{\sqrt{2}\cos(\frac{\phi}{2})}{\sqrt{1-\cos\phi + 2\cot^2(\theta+\triangle\theta)}}\right]. \quad (5)$$

Hence, the concise model for edge diffraction is expressed as follow, where the Green function $\mathrm{e}^{-\mathrm{j}kr}/r$ is omitted.

$$E^d_{\mathrm{V,H}} = \frac{L}{\pi}\mathrm{sinc}(2kL\cos\theta)\mathrm{F}_{\mathrm{V,H}}(\phi)\,\mathrm{e}^{\mathrm{j}2k\hat{s}\cdot\mathbf{r}'}. \quad (6)$$

Compared with (1) and (2) under VV polarization, the composite dependent functions on θ and ϕ are separated into single variable functions in (4) and (6). These functions are easier to operate in simulation and parameter estimation. Furthermore, (3) for HH polarization has been modified to (5) for better agreement with the numerical results computed by the full wave method. Besides, (4)–(6) further present the dependent functions on ϕ under different polarizations, whereas the aspect dependence on ϕ is not considered in the ASC model for edge diffraction. The validations of this model are presented in Appendix.

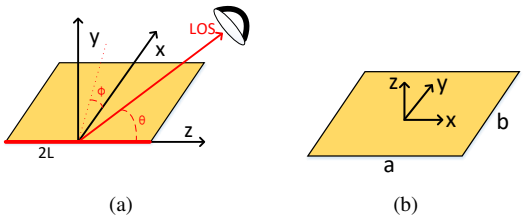

(a) (b)

Fig. 1. Geometry of the (a) edge on the half-planed and (b) flat plate.

2.2 The Scattering Center Model for Specular Reflection

According to the reflected fields (calculated by PO theory [20]) by a conducting rectangular plane situated at the origin as depicted in Fig. 1(b), the 3-D scattering center model for the distributed scattering center (DSC) of the plane can be expressed as:

$$E_{\mathrm{PO}} = \frac{\mathrm{j}kab\cos\theta}{2\pi}\mathrm{sinc}(ka\sin\theta\cos\phi) \\ \mathrm{sinc}(kb\sin\theta\sin\phi)\mathrm{e}^{\mathrm{j}2k\hat{s}\cdot\mathbf{r}'} \tag{7}$$

where a and b are length and width of the plane; $\mathbf{r}'$ is the location vector of the geometric center of the plane.

The scattering centers induced by straight edge diffractions and plane reflections are commonly taken as the same kind of DSC and described by the same aspect dependency function of sinc. However, their 3-D dependency functions are quite different from each other; they should be treated separately in the scattering center modeling by using different parameter models. The 3-D aspect dependencies on θ and ϕ of the scattering center induced by edge diffraction are presented in Fig. 12 and Fig. 14 in Appendix. In comparison, the 3-D aspect dependencies of the DSC of the plane are also given in Fig. 13. From Figs. 12–13, it can be seen that there are obvious differences between the aspect dependencies of edge diffractions and plane reflections.

3. Validations

Four conducting targets, two simple targets and two complex targets are investigated to validate these models. The two simple targets include a rectangular flat plane and a wing of an UAV. The complex targets include two propellers. These targets are concerned here because edge diffraction has been identified as the dominant scattering mechanisms to their total fields. For easier descriptions, the scattering centers are classified into three types referring to [14], the DSC, the localized scattering center (LSC), and the sliding scattering center (SSC).

To differentiate the DSCs induced by edge diffractions from the DSCs induced by plane reflections, they are denoted as DSC-D and DCS-R, respectively, in the following analysis. The RCS and TFR of scattered waves are compared in detail for these models (which is named as PTD-based model for short), PMLFMA and the ASC model. The frequency of incident plane waves is 3 GHz. The radar mode is monostatic.

3.1 Target A: Rectangular Plane

The rectangular plate with size of 1 m × 2 m lies in the x-z plane. The longer edges lie parallel to the z-axis. The geometry and the coordinate system are shown in Fig. 2. The observation angle is: $\theta = 90°$ $\phi \in [0°, 180°]$, with a step of 0.5°.

Within the given observation range, there are three observable DSCs on the plane: DSC-R, DSC-D1, and DSC-D2. DSC-R is induced by reflected waves; DSC-D1 and DSC-D2 are induced by edge diffractions. The contributions of the DSC-Ds can be calculated by (8).

In the case of HH polarization, except for the aforementioned scattering centers, the scattering center induced by surface travelling waves (denoted by TWSC) also contributes to the backscattered waves. The expression of the surface travelling waves is given in (10) referring to [21].

The corresponding parametric models for these scattering centers are described as follows.

$$E^{\mathrm{V,H}}_{\mathrm{DSC\text{-}D}i} = \frac{\mathrm{L}_i}{2\pi}F_{\mathrm{V,H}}(\phi-\phi_i,\theta_0)\mathrm{sinc}(2kL_i\cos\theta)\mathrm{e}^{\mathrm{j}2k\hat{s}\cdot\mathbf{r}'_i}, \\ i = 1,2 \tag{8}$$

$$E^{\mathrm{V,H}}_{\mathrm{DSC\text{-}R}} = \mathrm{j}A_3\sin\phi\mathrm{sinc}[2kL_3\cos\phi]\mathrm{e}^{\mathrm{j}2k\hat{s}\cdot\mathbf{r}'_3}, \tag{9}$$

$$E^{\mathrm{H}}_{\mathrm{TWSC}} = \mathrm{j}^{\alpha}A_4\sin^2\phi\mathrm{e}^{\mathrm{j}2k\hat{s}\cdot\mathbf{r}'_4} \\ \{\mathrm{sinc}[k(1+\cos\phi)] + \mathrm{sinc}[k(1-\cos\phi)]\} \tag{10}$$

where $L_{1,2}$ is the half length of the edge, L_3 is the half length of the projection of the plate onto the observation plane, $\phi_1 = 0°$ and $\phi_2 = 180°$, respectively, for the front and the back edges, $\mathbf{r}'_i$ are the locations of the ith scattering center, $A_3 = k/\pi$, the parameters α, A_4, and θ_0 are unknown reals that need to be estimated.

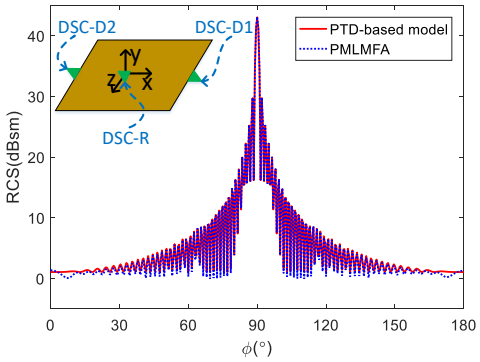

(a) VV polarization.

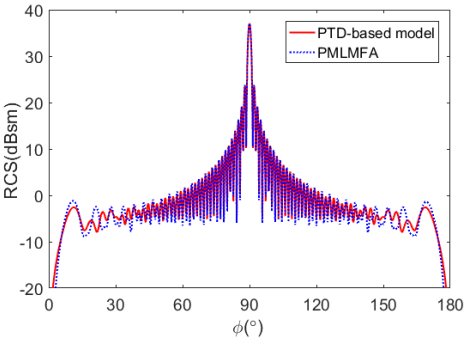

(b) HH polarization.

Fig. 2. The RCS results of the plane under two co-polarizations computed by the PTD-based model and PMLFMA.

Then, the total backscattered waves can be described by superimposing the contributions of all scattering centers. The unknown parameters of these models are estimated by genetic algorithm (GA) [22, 23] through matching the RCSs and the TFRs simulated by the PTD-based model with those computed by PMLFMA. The PC used here is Intel Core i7-4470 with 3.4 GHz. The 100 iterations in parameter estimation need about 200 minutes. To ensure the accuracy of estimation, two objective functions (OF) are employed in GA, as given below:

OF1: $y = -R(1;2) + 1$, where R is the matrix of correlation coefficient $R = \text{corrcoef}(TFR_\text{o}; TFR_\text{e})$. TFR_o and TFR_e indicate TFR of the backscattered waves computed by PMLFMA and the one simulated by described scattering center model respectively.

OF2: $y = \text{RMSE}(RCS_\text{o}; RCS_\text{e})$, where RMSE means the root-mean-square error; RCS_o and RCS_e indicate RCSs of the backscattered waves computed by PMLFMA and the one simulated by described scattering center model respectively.

The RCS results simulated by the PTD-based model and those by PMLFMA are presented in Fig. 2. It can be seen that the two results agree well with each other. The RMSEs of the two pairs of data under VV and HH polarizations are 0.5268 dB and 1.3737 dB respectively. The correlation coefficients are 99.86% and 98.33% respectively.

3.2 Target B: Wing of an UVA

The wing of an UVA is shown in Fig. 3. The simulation parameters, aspect angles are the same with the former case. The broadside of the wing is a trapezia with a height of 7 m, the longer width of 1 m and the shorter width of 0.5 m. The scattered waves under VV polarization is considered here.

Under the given observing angle range, there are four dominant scattering centers on the wing, as illustrated in Fig. 3. A DSC (denoted by DSC-D) is induced by diffraction of straight edge; two LSCs (denoted by LSC2, LSC3) are induced by the diffraction of the curved edges; Another DCS (denoted by DSC-R) is induced by reflected waves from the top plane of the wing. The corresponding parametric models of these scattering centers are described as follows:

$$E_\text{DSC-D} = A_1 F(\phi - \phi_1)\text{sinc}(2kL_1\cos\theta)\text{e}^{2\text{j}k\hat{s}\cdot\mathbf{r}'_1}, \tag{11}$$

$$E_{\text{LSC}i} = A_i \text{e}^{-\gamma_i|\sin(\phi-\phi_i)|}\text{e}^{2\text{j}k\hat{s}\cdot\mathbf{r}'_i}, \quad i = 2,3 \tag{12}$$

$$E_\text{DSC-R} = \text{j}A_4\sin\phi\,\text{sinc}(2kL_4\cos\phi)\text{e}^{2\text{j}k\hat{s}\cdot\mathbf{r}'_4} \tag{13}$$

where the parameters for DSC-D and DSC-R in (11) and (13) (A_1, A_4, L_1, L_4)can be calculated directly by the geometric parameters of the wing; the parameters for LSCs, A_i, γ_i and ϕ_i, need to be estimated.

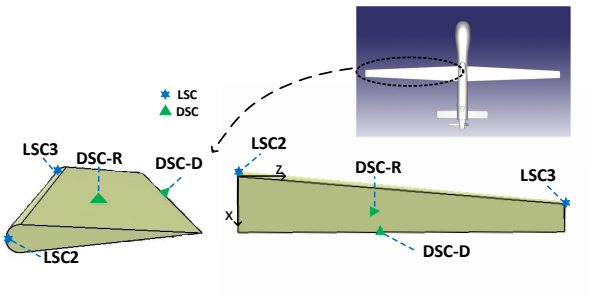

Fig. 3. The geometry of the wing and the observable scattering centers under the given observation range.

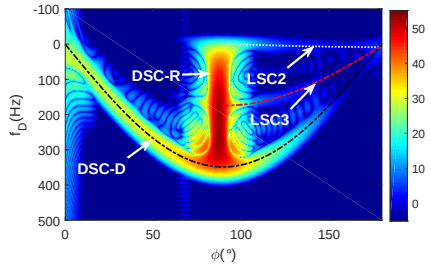

(a) The TFR computed by PMLFMA.

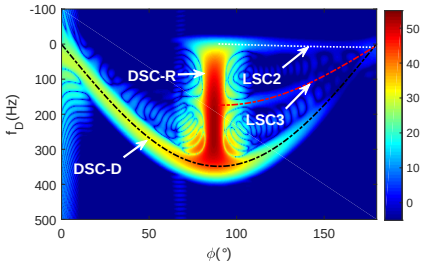

(b) The TFR simulated by the PTD-based model.

Fig. 4. The TFR of the scattered waves by the wing.

The TFR obtained by PMLFMA and the one simulated by the PTD-based model are presented in Fig. 4, where the four dominant scattering centers are also indicated. Figure 4 shows that the signatures of these dominant scattering centers described by the PTD-based model have achieved good agreements with those obtained by PMLFMA.

The comparison between the PTD-based model and ASC model is also given. In the ASC model, the function of aspect dependency for all different types of DSCs is all described by the sinc function, that is, the aspect dependency of the DSC induced by diffracted waves from the edge is the same model as for the waves induced by the reflection from the planar surface. The ASC model of the wing is presented as follows.

$$E_\text{DSC-D} = A_1\text{sinc}(2kL_i\cos\theta)\text{e}^{2\text{j}k\hat{s}\cdot\mathbf{r}'_1}, \tag{14}$$

$$E_{\text{LSC}i} = A_i \text{e}^{-\gamma_i|\sin(\phi-\phi_i)|}\text{e}^{2\text{j}k\hat{s}\cdot\mathbf{r}'_i}, \quad i = 2,3 \tag{15}$$

$$E_\text{DSC-R} = \text{j}A_4\text{sinc}(2kL_i\cos\phi)\text{e}^{2\text{j}k\hat{s}\cdot\mathbf{r}'_4} \tag{16}$$

where the parameters $(A_i, L_i, \gamma_i, \phi_i)$ in (14)–(16) need to be estimated.

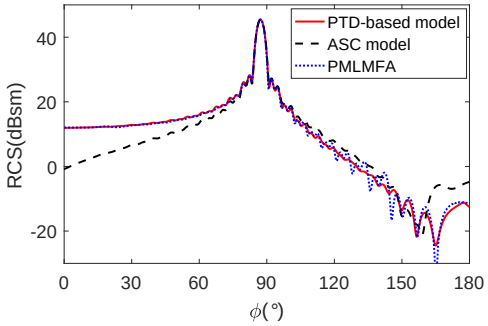

Fig. 5. The RCS results of the wing simulated by the PTD-based model, the ASC model and PMLFMA.

The comparisons of RCSs obtained by three methods, the PTD-based model, the ASC model and PMLFMA, are shown in Fig. 5. It can be seen that the PTD-based model has higher precision than the ASC model in characterizing the fluctuations of RCS, especially in the range $\phi = 0° \sim 120°$. The RCSs in the range $\phi = 120° \sim 180°$ are not that good as other aspect angles because the scattered waves are contributed mainly by the two LSCs, and they are describe by the commonly used damped exponential model. Statistic results about correlation coefficients of the simulated TFRs with that of PMLFMA and the RMSE of the simulated RCSs with those of PMLFMA are listed in Tab. 1.

3.3 Target C: Three-Blade-Propeller of Helicopter

The geometry of one the propeller is shown in Fig. 6. The propeller has three blades, and the shape of each blade is a long, narrow rectangular plate with a size of 3 m × 0.25 m. The back edge of the three blades lie in xoz plane. The angle between the each blade and the xoz plane is 0°. The observation angle is: $\theta = 90°$, $\phi = 0° \sim 180°$, with a step of 0.25°. The scattered waves under VV polarization is considered here.

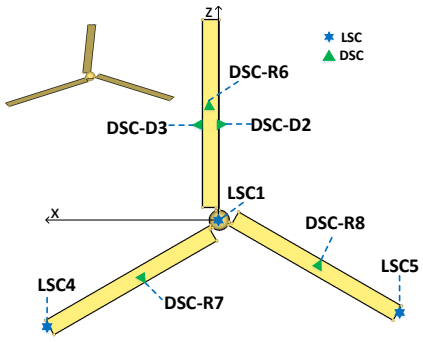

Fig. 6. The geometry of the three-blade-propeller and the observable scattering centers under the given observation range.

Under the given observation range, there are eight dominant scattering centers, as illustrated in Fig. 6. Three LSCs (denoted by LSC1, LSC4, LSC5), are induced by diffracted waves from the blade tips and the small spherical axle. The locations of these three LSCs are the tips of blades and the center of the spherical axle respectively. Two DSCs (denoted by DSC-D2, DSC-D3) are induced by diffracted waves from the straight edges. Three DSCs (denoted by DSC-R6, DSC-R7 and DSC-R8) are induced by reflected waves from the planes of the blades.

According to the PTD-based model, the diffracted contributions of DSC-Ds can be calculated by (18), and the reflected contributions of DSC-Rs can be simulated by (19). LSC1 is simulated by the ideal scattering center model according the scattering characteristics of specularly reflected waves by the sphere. The corresponding parametric models for these scattering centers are described as follows:

$$E_{\text{LSC}i} = \mathrm{j}^{\alpha_i} A_i \mathrm{e}^{-\gamma_i |\sin(\phi-\phi_i)|} \mathrm{e}^{2\mathrm{j}k\hat{s}\cdot\mathbf{r}'_i}, \quad i = 1, 4, 5 \tag{17}$$

$$E_{\text{DSC-D}i} = A_i F(\phi-\phi_i)\mathrm{sinc}(2kL_i\cos\theta)\mathrm{e}^{2\mathrm{j}k\hat{s}\cdot\mathbf{r}'_i}, \quad i = 2, 3 \tag{18}$$

$$E_{\text{DSC-R}i} = \mathrm{j}A_i \sin\phi \mathrm{sinc}(2kL_i\cos\phi)\mathrm{e}^{2\mathrm{j}k\hat{s}\cdot\mathbf{r}'_i}, \quad i = 6, 7, 8 \tag{19}$$

where the parameters (A_i and L_i) for DSC-Ds and DSC-Rs in (18) and (19) can be calculated directly by the geometric parameters of the propeller; the parameters for LSCs in (17) need to be estimated.

For comparison, the ASC model of this target is also given:

$$E_{\text{LSC}i} = \mathrm{j}^{\alpha_i} A_i \mathrm{e}^{-\gamma_i |\sin(\phi-\phi_i)|} \mathrm{e}^{2\mathrm{j}k\hat{s}\cdot\mathbf{r}'_i}, \quad i = 1, 4, 5 \tag{20}$$

$$E_{\text{DSC-D}i} = A_i \mathrm{sinc}(2kL_i\cos\theta)\mathrm{e}^{2\mathrm{j}k\hat{s}\cdot\mathbf{r}'_i}, \quad i = 2, 3 \tag{21}$$

$$E_{\text{DSC-R}i} = jA_i \mathrm{sinc}(2kL_i\cos\phi)\mathrm{e}^{2\mathrm{j}k\hat{s}\cdot\mathbf{r}'_i}, \quad i = 6, 7, 8 \tag{22}$$

where the parameters ($A_i, L_i, \gamma_i, \phi_i$) in (20) ~ (22) need to be estimated.

The TFR of backscattered waves computed by PMLFMA and those simulated by the PTD-based model are presented in Fig. 7, where the corresponding signatures of scattering centers are indicated. It can be seen that the signatures of the scattering centers characterized by the PTD-based model have achieved good agreements with the results of PMLFMA.

The comparisons of RCSs obtained by three methods, the PTD-based model, the ASC model and PMLFMA, are shown in Fig. 8. It can be seen that the PTD-based model has better agreement than the ASC model in characterizing the fluctuations of RCS. Statistic results about correlation coefficients of the simulated TFRs with that of PMLFMA and the RMSE of the simulated RCSs with those of PMLFMA are given in Tab. 1.

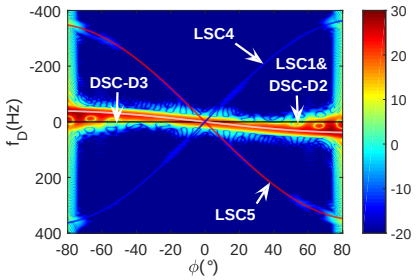

(a) The TFR computed by PMLFMA.

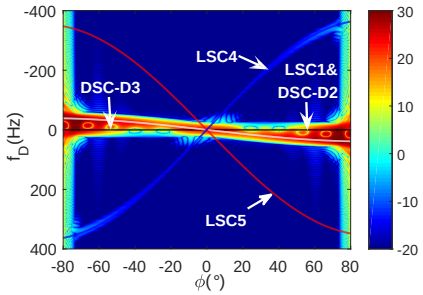

(b) The TFR simulated by the PTD-based model.

Fig. 7. The TFR of the scattered waves by the three-blade-propeller.

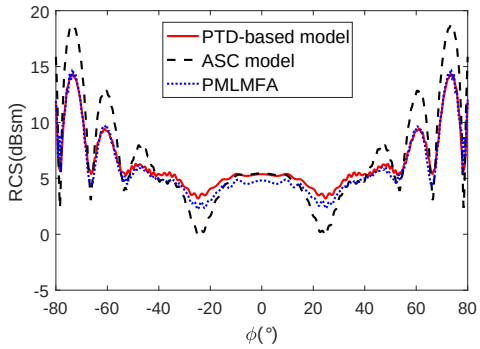

Fig. 8. The RCS results of the three-blade-propeller simulated by the PTD-based model, the ASC model and PMLFMA.

3.4 Target D: Four-Blade-Propeller of Helicopter

The geometry of the propeller with four blades is shown in Fig. 15. The back edge of the four blades lie in xoz plane. The angle between the each blade and the xoz plane is 15°.The blades are with size of 2.5 m × 0.3 m. The aspect angles are $\theta = 0°, \phi = 0 \sim 180°$, with a step of 0.25°. The scattered waves under VV polarization is considered here.

According to the geometry of propeller and the given observation angles, nine observable scattering centers can be predicted: including a LSC induced by the spherical reflection, denoted by LSC1; four DSC-Ds induced by the edge diffraction, denoted by DSC-D2, DSC-D3, DSC-D4, DSC-D5; four DSCs generated by specular reflections of blades, denoted by DSC-R6, DSC-R7, DSC-R8 and DSC-R9.

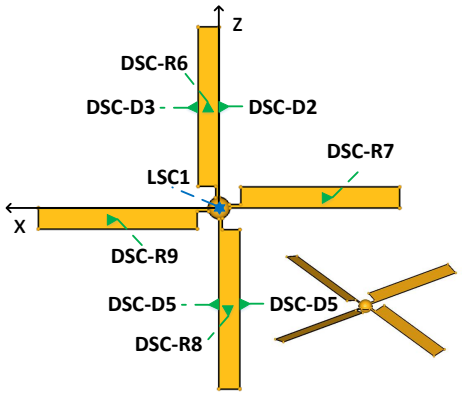

Fig. 9. The geometry of the four-blade-propeller and the observable scattering centers under the given observation range.

The scattering center models for the propeller can be described as follows.

$$E_{\text{LSC1}} = A_1 \mathrm{e}^{2\mathrm{j}k\hat{s}\cdot\mathbf{r}'_1}, \tag{23}$$

$$E_{\text{DSC-D}i} = A_i F(\phi - \phi_i)\text{sinc}(2kL_i\cos\theta)\mathrm{e}^{2\mathrm{j}k\hat{s}\cdot\mathbf{r}'_i}, \quad i = 2, 3, \ldots, 5 \tag{24}$$

$$E_{\text{DSC-R}i} = \mathrm{j}A_i \sin\phi\,\text{sinc}(2kL_i\cos\phi)\mathrm{e}^{2\mathrm{j}k\hat{s}\cdot\mathbf{r}'_i} \quad i = 6, 7, \ldots, 9 \tag{25}$$

where the parameters (A_i and L_i) of DSC-Ds and DSC-Rs in (24) and (25) can be calculated directly by the geometric parameters of the propeller; the parameters for LSC1 need to be estimated.

The ASC model of the wing is also given, as follows:

$$E_{\text{LSC1}} = A_1 \mathrm{e}^{2\mathrm{j}k\hat{s}\cdot\mathbf{r}'_1}, \tag{26}$$

$$E_{\text{DSC-D}i} = A_i \text{sinc}(2kL_i\cos\theta)\mathrm{e}^{2\mathrm{j}k\hat{s}\cdot\mathbf{r}'_i}, \quad i = 2, 3, \ldots, 5 \tag{27}$$

$$E_{\text{DSC-R}i} = \text{æ}A_i \text{sinc}(2kL_i\cos\phi)\mathrm{e}^{2\mathrm{j}k\hat{s}\cdot\mathbf{r}'_i}, \quad i = 6, 7, \ldots, 9 \tag{28}$$

where the parameters (A_i, L_i) of (26)–(28) need to be estimated.

The TFRs computed by the PTD-based model and PMLFMA are shown in Fig. 10. The RCSs computed by the two models are shown in Fig. 11, together with that by PMLFMA. Statistic results about correlation coefficients of the simulated TFRs with that of PMLFMA and the RMSE of the simulated RCSs with those of PMLFMA are listed in Tab. 1. It can be seen that this model has higher precision in simulating TFR and RCS than the ASC model.

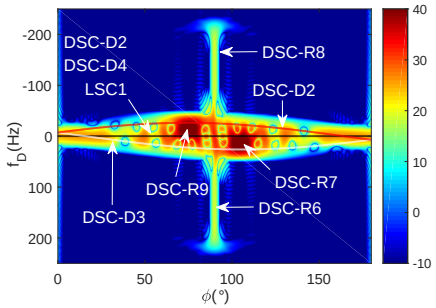

(a) The TFR computed by PMLFMA.

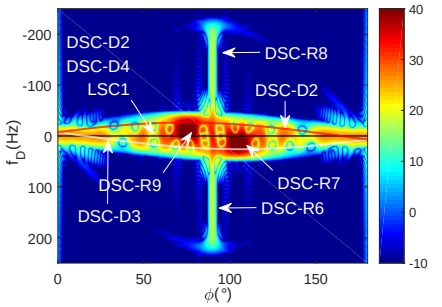

(b) The TFR simulated by the PTD-based model.

Fig. 10. The TFR of the scattered waves by the four-blade-propeller.

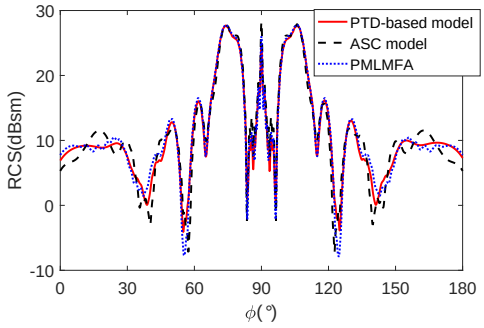

Fig. 11. The RCS results of the four-blade-propeller simulated by the PTD-based model, the ASC model and PMLFMA.

	Target	This model	ASC model
CorrCoef of TFR	B	96.11%	93.74%
	C	96.56%	95.45%
	D	96.55%	93.49%
RMSE of RCS	B	0.62 dB	5.78 dB
	C	1.49 dB	6.66 dB
	D	1.12 dB	2.49 dB

Tab. 1. Statistic results of correlation coefficient of TFR and the RMSE of RCS.

4. Conclusions

A modified scattering center model based on solutions of PO and EEC instead of PO and GTD is presented in this work. By doing this, the problems included by the similarities of GTD and duplicated scattering components of reflections and diffractions are avoided. Compared with the existing models, the PTD-based model can characterize the scattered fields under 3-dimensional aspect angles and arbitrary polarizations with better accuracy, especially for diffraction contributions. And its parameters are related directly to the geometry of the target, which bring much convenience for applications.

Four exemplary targets with dominant scattering centers induced by diffraction are investigated to validate this model. RCS and TFR results which were obtained by this model, PMLFMA and the ASC model are presented for comparison. The results demonstrate that the simulation results of RCS and TFR by using this model have achieved higher accuracies than the ASC model.

Acknowledgments

This work was supported by the National Natural Science Foundation of China (grant No. 61471041 and 61771052).

References

[1] KELLER, J. B. Geometrical theory of diffraction. *Journal of the Optical Society of America*, 1962, vol. 52, no. 2, p. 116–130.

[2] HURST, H. P., MITTRA, R. Scattering center analysis via Prony's method. *IEEE Transactions on Antennas and Propagation*, 1987, vol. 35, no. 8, p. 986–988. DOI: 10.1109/TAP.1987.1144210

[3] POTTER, L. C., CHIANG, D. M., CARRIERE, R., et al. GTD-based parametric model for radar scattering. *IEEE Transactions on Antennas and Propagation*, 1995, p. 1058–1067. DOI:10.1109/8.467641

[4] GERRY, M. J., POTTER, L. C., GUPTA, I. J., et al. A parametric model for synthetic aperture radar measurements. *IEEE Transactions on Antennas and Propagation*, 1999, vol. 47, no. 7, p. 1179–1188. DOI: 10.1109/8.785750

[5] GUO, K. Y., LI, Q. F., SHENG, X. Q. Sliding scattering center model for extended streamlined targets. *Progress In Electromagnetics Research*, 2013, vol. 139, no. 3, p. 499–516. DOI:10.1109/8.467641

[6] QU, Q. Y., GUO, K. Y., SHENG, X. Q. An accurate bistatic scattering center model for extended cone-shaped targets. *IEEE Transactions on Antennas and Propagation*, 2014, vol. 62, no. 10, p. 5209–5218. DOI:10.1109/TAP.2014.2342761

[7] QU, Q. Y., GUO, K. Y., SHENG, X. Q. Scattering centers induced by creeping waves on cone-shaped targets in bistatic mode. *IEEE Transactions on Antennas and Propagation*, 2015, vol. 63, no. 7, p. 3257–3262. DOI:10.1109/LAWP.2014.2367510

[8] FENG, Z., YING, L., QUN, Z., et al. ISAR imaging for avian species identification with frequency-stepped chirp signals. *IEEE Geoscience and Remote Sensing Letters*, 2010, vol. 7, no. 1, p. 151–155. DOI: 10.1109/LGRS.2009.2028902

[9] ZHOU, J. X., SHI, Z. G., CHENG, X., et al. Automatic target recognition of SAR images based on global scattering center model. *IEEE Transactions on Geoscience and Remote Sensing*, 2011, vol. 49, no. 10, p. 3713–3729. DOI: 10.1109/TGRS.2011.2162526

[10] DIEMUNSCH, J. R. Moving and stationary target acquisition and recognition (MSTAR) model-based automatic target recognition: Search technology for a robust ATR. *Algorithms for Synthetic Aperture Radar Imagery V*, 1998, vol. 3370, no. 1, p. 481–192. DOI: 10.1109/TGRS.2011.2162526

[11] ZHOU, J., ZHOU, H., FU, Q. Global scattering center model extraction of radar targets based on wideband measurements. *IEEE Transactions on Antennas and Propagation*, 2008, vol. 56, no. 7, p. 2051–2060. DOI: 10.1109/TAP.2008.924698

[12] RIGLING, B. D., CHENG, R. L. Three-dimensional surface reconstruction from multistatic SAR images. *IEEE Transactions on Image Processing*, 2005, vol. 14, no. 8 p. 1159–1171. DOI: 10.1109/TIP.2005.851690

[13] GUO, K. Y., QU, Q. Y., SHENG, X. Q. Geometry reconstruction based on attributes of scattering centers by using time-frequency representations. *IEEE Transactions on Antennas and Propagation*, 2005, vol. 14, no. 2, p. 1159–1171. DOI: 10.1109/TAP.2015.2511779

[14] KNOTT, E. F. Comparison of three high-frequency diffraction techniques. *Proceedings of the IEEE*, 1974, vol. 62, no. 11, p. 1468–1474. DOI: 10.1109/PROC.1974.9653

[15] MICHAELI, A. Elimination of infinities in equivalent edge currents, Part I: fringe current component. *IEEE Transactions on Antennas and Propagation*, 1986, vol. 34, no. 7, p. 912–918. DOI: 10.1109/TAP.1986.1143913

[16] PAN, X. M., SHENG, X. Q. A sophisticated parallel MLFMA for scattering by extremely large targets. *IEEE Antennas and Propagation Magazine*, 2008, vol. 50, no. 3, p. 129–138. DOI: 10.1109/MAP.2008.4563583

[17] GUO, K. Y., SHENG, X. Q. Miss distance estimation based on scattering center model using time-frequency analysis. *IEEE Antennas and Wireless Propagation Letters*, 2015, vol. 15, no. 10, p. 1012–1015. DOI: 10.1109/LAWP.2015.2490088

[18] AUGER, F., FLANDRIN, P. Improving the readability of time frequency and time scale representations by the reassignment method. *IEEE Transactions on Signal Processing*, 2006, vol. 52, no. 2, p. 489–509. DOI:10.1109/78.382394

[19] MICHAELI, A. Equivalent edge currents for arbitrary aspects of observation. *IEEE Transactions on Antennas and Propagation*, 1984, vol. 32, no. 3, p. 252–258. DOI:10.1109/TAP.1984.1143303

[20] KNOTT, E. F. RCS reduction of dihedral corners. *IEEE Transactions on Antennas and Propagation*, 1977, vol. 25, no. 3, p. 406–409. DOI: 10.1109/TAP.1977.1141586

[21] KNOTT, E. F., SHAEFFER, J. F., TULEY, M. T. *Radar Cross Section*. Scitech Publishing, 2004. ISBN: 1891121251

[22] LI, Q., ROTHWELL, E. J., CHEN, K. M., et al. Scattering center analysis of radar targets using fitting scheme and genetic algorithm. *IEEE Transactions on Antennas and Propagation*, 1996, vol. 44, no. 2, p. 198–207. DOI:10.1109/8.481648

[23] HUGHES, E. J., LEYLAND, M. Using multiple genetic algorithms to generate radar point-scatterer models. *IEEE Transactions on Evolutionary Computation*, 2000, vol. 4, no. 2, p. 147–163. DOI:10.1109/4235.850655

About the Authors . . .

Xiao-Tong ZHAO was born in 1992. She received her B.S. degree from Beijing Institute of Technology in 2014. Her research interests include electromagnetic simulation, radar feature extraction, and radar signal processing.

Kun-Yi GUO received her the Ph.D. degree in Electromagnetics and Microwave Technology from the Institute of Electronics, Chinese Academy of Sciences, in 2005. Her research interests include electromagnetic simulation, microwave imaging, and radar signal processing.

Xin-Qing SHENG received the B.S., M.S., and Ph.D. degrees from the University of Science and Technology of China (USTC), Hefei, China, in 1991, 1994, and 1996, respectively. His research interests include computational electromagnetics, scattering and antenna analysis, electromagnetic compatibility, and microwave imaging.

Appendix

Equations (4)–(6) have been validated by a series of numerical results, as presented below. The diffracted fields (under VV and HH polarizations) computed by the model are compared with the original EEC formula in Fig. 12 and Fig. 14, and the differences between them are also given. The parameters used in computations are: $L = 1$; $f = 3\,\text{GHz}$, $\triangle\theta = 4.3°$, $\theta \in [0°, 180°], \phi \in [0°, 180°]$. The differences under VV polarization are very small as shown in Fig. 12(c). The relative differences under VV polarization are less than 0.01.

Due to the modification we made under HH polarization, there are larger differences between the two results within some observation angles as shown in Fig. 14(c). To demonstrate the higher accuracy of the modified expression, the RCS results under HH polarization of a conducting plate (with length $a = 2\,\text{m}$ and width $b = 2\,\text{m}$) computed by the model are compared with those computed by the EEC formula and PMLFMA. The observation angles are set as $\theta = 90°, \phi \in [0°, 180°]$ at $f = 3\,\text{GHz}$. The RMSEs of the two pairs of results are 2.3335 dB and 4.1208 dB, respectively.

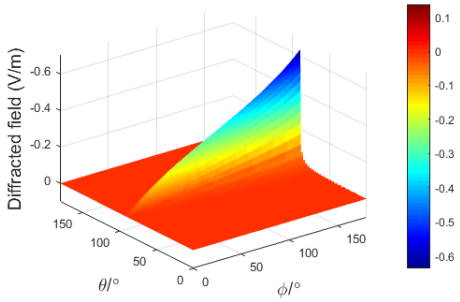

(a) EEC formula.

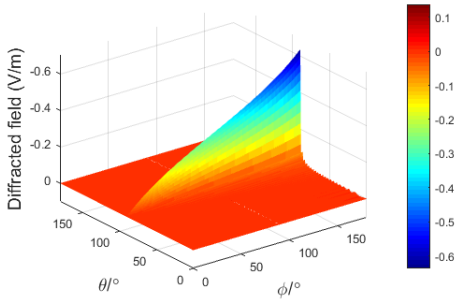

(b) This model.

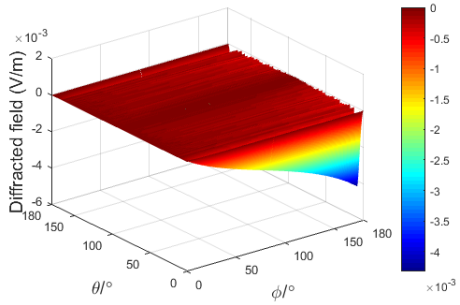

(c) The differences between the model and the original EEC formula.

Fig. 12. The diffracted fields computed by the model and the original EEC formula under VV polarization.

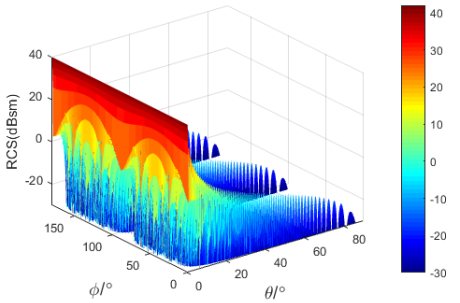

Fig. 13. 3-D aspect dependencies of the scattering center induced by plate reflection ($a = 2$ m, $b = 1$ m).

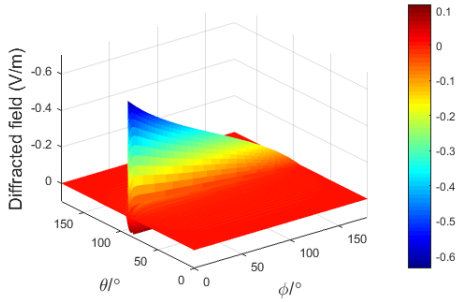

(a) EEC formula.

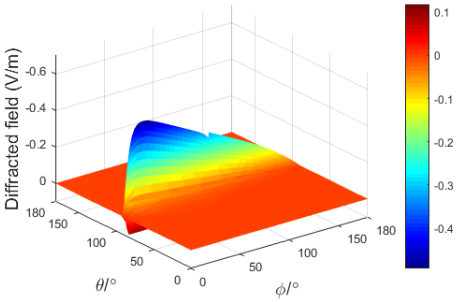

(b) This model.

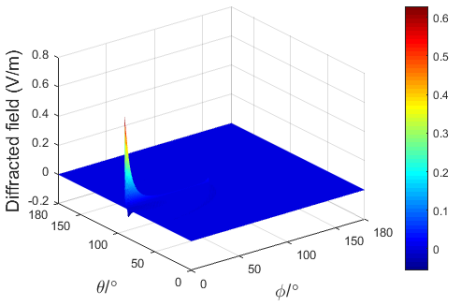

(c) The differences between the model and the original EEC formula.

Fig. 14. The diffracted fields computed by the model and the original EEC formula under HH polarization.

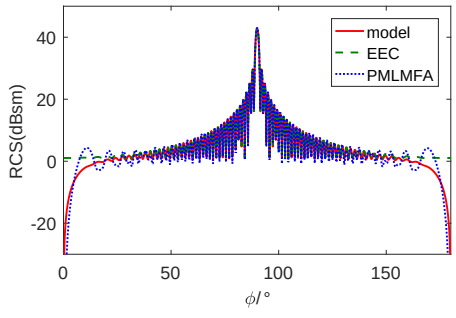

Fig. 15. The RCS results of the plate under HH polarizations computed by this model ($\triangle\theta = 4.3°$), the EEC formula and PMLFMA.